J. Appl. Comput. Mech., 10(4) (2024) 652-658
DOI: 10.22055/jacm.2024.45493.4377

ISSN: 2383-4536
jacm.scu.ac.ir

Shahid Chamran University of Ahvaz

Journal of Applied and Computational Mechanics

Research Paper

An Efficient Ply-Level Based Modeling Strategy for Predicting Delamination Behavior in Laminated Composites

Khairul Anam[1], Melanie Todt[2], Heinz E. Pettermann[2]

[1] Department of Mechanical Engineering, Brawijaya University, Jl. MT Haryono 167, Malang 65145, Indonesia, Email: khairul.anam27@ub.ac.id

[2] Institute of Lightweight Design and Structural Biomechanics, TU Wien, Getreidemarkt 9, 1060 Vienna, Austria,
Email: melanie.todt@tuwien.ac.at (M.T.); heinz.pettermann@tuwien.ac.at (H.E.P.)

Received December 07 2023; Revised February 26 2024; Accepted for publication April 04 2024.
Corresponding author: K. Anam (khairul.anam27@ub.ac.id)
© 2024 Published by Shahid Chamran University of Ahvaz

Abstract. A ply-level based modeling strategy for predicting the delamination behavior of laminated composites under pure and mixed mode loading conditions is implemented within the framework of the Finite Element Method. Each ply and each interface of the laminate is explicitly modeled, with the plies represented by various element types such as conventional shell, continuum shell, and continuum elements, and the interfaces are discretized using cohesive zone elements. The comparison between all models is examined in terms of delamination onset and growth including load-displacement curves, delamination area, computation time, and mode-mixity. The results show that all ply-level based modeling strategies exhibit very good agreement with the analytical results. Moreover, ply-level approach based on shell elements in combination with finite thickness cohesive zone elements offers a numerically efficient simulation tool to predict delamination behavior in laminates.

Keywords: Laminates, Layered Structures, Delamination, Finite Element Analysis (FEA).

1. Introduction

Delamination is one of the major failure mechanisms that usually occurs in laminated composites. Mostly, delamination occurs internally, so, the damage cannot be seen by the naked eye on the composite surface and is difficult to detect during service. Predominantly, the damage produced by the delamination results in decreases of strength, fracture toughness, and fatigue-life [1]. Delamination to occur requires a sufficient magnitude of local tractions at the ply-to-ply interfaces. When a laminated shell is mainly loaded in plane, interface tractions can be caused by free edge effects, ply drop off, geometrical features, and pronounced curvature of the structure [2, 3]. Additionally, traction can be caused by transverse loads and impact scenarios.

The delamination behavior of laminated composites has received a significant attention in the last few decades treated by both experimental and numerical methods. Experimental schemes are usually employed for characterizing the delamination resistance of laminated composites, namely the critical strain energy release rate or the inter-laminar fracture toughness. Common experimental set-ups for observing the delamination behavior under mode I (opening mode) and mode II (shear mode) loading scenarios are double cantilever beam (DCB) and end notch flexure (ENF) tests, respectively [4]. For the mode I/II (mixed-mode) loading scenario, several types of test set-ups are used including single-leg bending (SLB), over-leg bending (OLB), cracked-lap shear (CLS), and mixed-mode flexure (MMF) tests. However, experimental methods are often less efficient, expensive, and rarely used to test large scale and complex laminated composites structures. There, numerical methods based on the Finite Element Method (FEM) provide a method for predicting the delamination behavior of laminated composites. Not only linear case, but numerical methods are also capable to estimate the nonlinear mechanical response at various length scales under various loading conditions [5]. Nevertheless, the investigation of local effects such as delamination in a composites structure is demanding in terms of computation resources. Consequently, the need for a modeling strategy that has high computational efficiency, high reliability, and wide application coverage such as various length scale and various loading condition is needed.

A Cohesive Zone Model (CZM) is a common approach that has been applied to investigate the delamination behavior which has been first introduced by Dugdale [6] and Barenblatt [7]. The CZM has been implemented frequently in FEM analysis to simulate the delamination of laminated components [8-11], as well as debonding [12], and crack propagation [13]. Furthermore, it has been demonstrated to have considerable computational efficiency [9]. Heidari-Rarani and Sayedain [14] also found that CZM is the most efficient compared to other methods such as Virtual Crack Closure Technique (VCCT), Extended Finite Element Method (XFEM)-VCCT, and XFEM-CZM for both two-dimensional (2D) and three-dimensional (3D).

Many researchers used the CZM for investigation the delamination in laminates for the sake of computational efficiency. However, for large scale and complex laminates, the need for a method to save computational time without compromising reliable

Published online: April 10 2024

results are still special of interest. The fundamental idea behind this research is that if a small amount of computation time can be saved for simple models, a lot of computation time can be saved for large and complex structures. In this research, various ply-level modeling strategy based on CZM are used to investigate the delamination behavior of the laminated composites where each ply and interface is explicitly modeled. This strategy has been extensively applied by utilizing different types of elements for the plies which are connected by cohesive zone elements (CZEs). Various ply-level modeling strategies have been reported in [15] and are illustrated in Fig. 1 where only one interface with its adjacent plies is shown. Figure 1(a) presents a combination between shell elements and finite geometrical thickness CZEs for the plies and the interfaces, respectively, that are connected by shared node coupling at the midplanes of plies. It has to be noted that even if the finite geometrical thickness CZE is used for the interfaces, the CZEs model the mechanical behavior of a zero-thickness interface. This is because a traction-separation based constitutive law is applied [9]. Furthermore, by using the share node coupling method, the thickness of the CZE is equal to ply thickness. Figure 1(b-d) presents a combination between conventional shell, continuum shell, and continuum elements and a zero thickness CZE for the plies and the interfaces, respectively, that are connected by utilizing surface-to-surface tie constraints.

The aim and scope of this study is to investigate and compare several ply-level modeling strategies for predicting the delamination behavior of laminated composites under pure and mixed mode loading conditions by the means of the Finite Element Method. Analytical results based on Corrected Beam Theory (CBT) (see Appendix) serve as the reference result. The comparison between all proposed models is examined in terms of delamination response including load-displacement curves, delamination area, computation time, and mode-mixity during delamination propagation.

2. Numerical Methods

All FEM computations are conducted using Abaqus/Standard 2020 [16] where an implicit solution scheme is applied to account for geometrically nonlinear behavior and progressive damage and failure of the interfaces.

2.1. Geometrical Modeling

The geometrical modeling of the double cantilever beam (DCB), end-notch flexure (ENF), and single-leg bending (SLB) set-ups is shown in Fig. 2. The laminated composites are made up of eight plies, with CZEs connecting all adjacent plies. Every ply has 949 elements where each element has element has a length of l_x, l_y, and l_z are 0.158125 mm, 1.0 mm, and 0.31625 mm, respectively. Furthermore, fully integrated and linearly interpolated elements are employed for the SPLF, SPLZ, and CPLZ configurations whereas reduced integrated linear elements are used for CSPLZ configuration. The normal direction of the orientation of the plies is in the positive z-direction. As shown in Fig. 2, the initial delamination, a, for the ENF and SLB are set to be greater than for the DCB and should be at least 0.7 times the length L to maintain stability of the delamination growth [17, 18]. Plane strain boundary conditions in y-direction, i.e., $\varepsilon_{yy} = \gamma_{xy} = \gamma_{yz} = 0$, are imposed to mimic the situation in a structure sufficiently apart from free edges. Additionally, as large deformations are being considered in the simulation, geometric nonlinear analysis is carried out. For all setups, a total displacement of 20 mm is used at a rate of 0.005 mm/s.

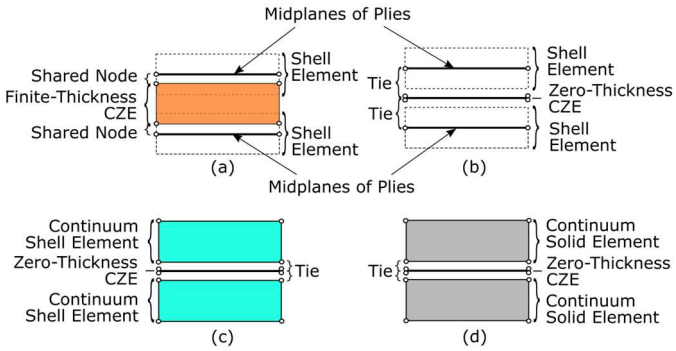

Fig. 1. The illustration of the ply-level based modeling strategy by combining; (a) conventional shell elements with finite thickness CZE denoted as SPLF, and (b) shell, (c) continuum shell, (d) continuum elements with zero thickness CZE denoted as SPLZ, CSPLZ, CPLZ, respectively.

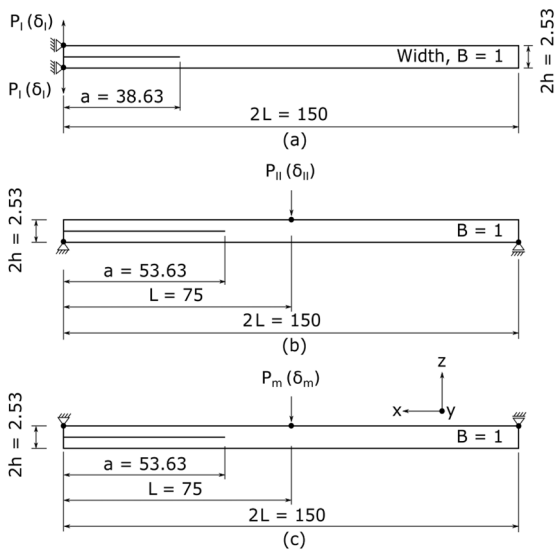

Fig. 2. The geometrical modeling of the (a) DCB, (b) ENF, and (c) SLB set-ups (dimensions in mm) [5].

Table 1. Ply properties of homogenized carbon/epoxy 2×2 twill weave composite material [19, 20].

Properties	Value
Young's modulus in x – direction, E_x	56589.32 (N/mm^2)
Young's modulus in y – direction, E_y	56589.32 (N/mm^2)
Young's modulus in z – direction, E_z	10066 (N/mm^2)*
Shear modulus, $G_{xy} = G_{xz} = G_{yz}$	4185.86 (N/mm^2)
Poisson's ratio, ν_{xy}	0.045
Poisson's ratio, $\nu_{xz} = \nu_{yz}$	0.33*

* Only apply to CPLZ

Table 2. Interface properties.

Mode I	Mode II
K_I = 10^5 (N/mm^3)	K_{II} = 10^5 (N/mm^3)
t_n^0 = 60 (N/mm^2)	t_s^0 = 79.289 (N/mm^2)
$\mathcal{G}_{IC}$ = 0.9 (N/mm)	$\mathcal{G}_{IIC}$ = 2.0 (N/mm)

2.2. Material Properties

The properties of the plies in Table 1 are obtained from [19, 20]. Damage initiation of the CZEs is expected to occur when a quadratic interaction function with nominal stress ratios reaches a value of one [16]. This criterion can be expressed as follows:

$$\left\{\frac{\langle t_n \rangle}{t_n^0}\right\}^2 + \left\{\frac{t_s}{t_s^0}\right\}^2 \geq 1 \tag{1}$$

where, t_i are the normal, *n*, and shear, s, component of the traction vector and t_i^0 are the corresponding interlaminar strengths. Damage evolution is modeled based on the critical energy release rates in combination with a linear softening law. The Benzeggagh and Kenane (BK) criterion is used to treat mixed mode behavior [21]. The BK law model for 2D mixed mode case gives the critical energy release rate,

$$\mathcal{G}_{equivC} = \mathcal{G}_{IC} + (\mathcal{G}_{IIC} - \mathcal{G}_{IC})(\psi)^{\eta} \tag{2}$$

$$\psi = \frac{\mathcal{G}_{II}}{\mathcal{G}_I + \mathcal{G}_{II}} \tag{3}$$

where, $\mathcal{G}_{IC}$ are the fracture toughness values, ψ is the mode-mixity, and $\mathcal{G}_I$ describe the work done by the pure mode tractions t_i on the corresponding separations δ_i, and η is a mixed mode parameter obtained from experiments. In this study, the mixed mode parameter, η is of 1.75 [2]. The interface properties in Table 2 define the initial stiffnesses, K, together with inter-laminar strengths, t [5] and the critical energy release rates, $\mathcal{G}_{iC}$ [22].

2.3. Contact Modeling

The contact constraints within the ENF and SLB simulation are enforced using the surface-to-surface contact algorithm of Abaqus/Standard, which utilizes a frictionless contact definition to prevent inter-ply penetration in regions of delamination. A hard contact penalty algorithm is also applied in which the penalty stiffness value is 42.5 % less than the representative underlying element stiffness. Additionally, viscous regularization with a 10^{-4} s relaxation time and adaptive automatic stabilization are utilized to improve the convergence of the simulations. The default value of 2.0 × 10^{-4} is chosen for the dissipated energy fraction, and the accuracy tolerance of 0.05 is utilized for the automatic damping algorithm [16].

3. Results and Discussion

The results of this study are completely achieved by means of numerical simulations. All set-ups are run on a single personal computer (PC) with eight CPUs ranging from 2.35 to 3.35 GHz.

3.1. Load-Displacement Curve

Figure 3 illustrates the load-displacement predictions of the (a) DCB, (b) ENF, and (c) SLB set-ups. In general, the load-displacement curves of all simulation set-ups correspond very well with the CBT results. The predicted pre-peak stiffness and the maximum load of the SPLF for the DCB simulations are slightly higher than for the other models. The higher stiffness is mainly generated by the finite thickness of the CZEs and the high stiffness assigned to the CZEs. The CSPLZ is the only one having a different delamination behavior for the ENF load-displacement results. After the maximum load is reached, the delamination does not propagate immediately. The maximum load, on the other hand, is comparable to the other models. For the SLB simulations result, all models can accurately predict the delamination behavior in laminated composites under mixed mode loading conditions. The load decreases when the delamination starts to propagate and then increases when the displacement reaches 17.5 mm. This increase in load occurs when the delamination reaches the load point. The delamination beyond the load point propagates more slowly and is dominated by mode II delamination.

3.2. Delamination Area and Computation Time

Figure 4 presents the process zones and delamination areas of different ply-level models which is represented by the stiffness degradation (SDEG) distribution on the CZEs in front of the initial delamination. Figure 4(a) presents the process zones at the maximum load, just before the delamination begins to propagate. To ensure the accuracy of the modeling of delamination propagation, the process zone near the delamination tip must be well resolved. Falk et al. [23] demonstrated that four to ten elements inside the process zones are adequate to predict the propagation of delamination. The number of elements in the process zones for the proposed ply-level models ranges between seven and nine elements. Figure 4(b) shows the process zones at the maximum displacement as well as the delamination areas (shown in light grey regions). The light grey elements represent the fully damaged of CZEs that reach an SDEG value of 0.9999. In Fig. 4(b), an SDEG of 0.9999 was chosen instead of 1 to simplify the way of visualizing and measuring the delamination area. According to the process zone, a value of 0.9999 is sufficient to represent fully damaged of the layer where the process zone at the maximum load and the end of the loading event are the same. Figure 4(c) highlights the SDEG of the SPLF model at maximum load and maximum displacement along the x-axis.

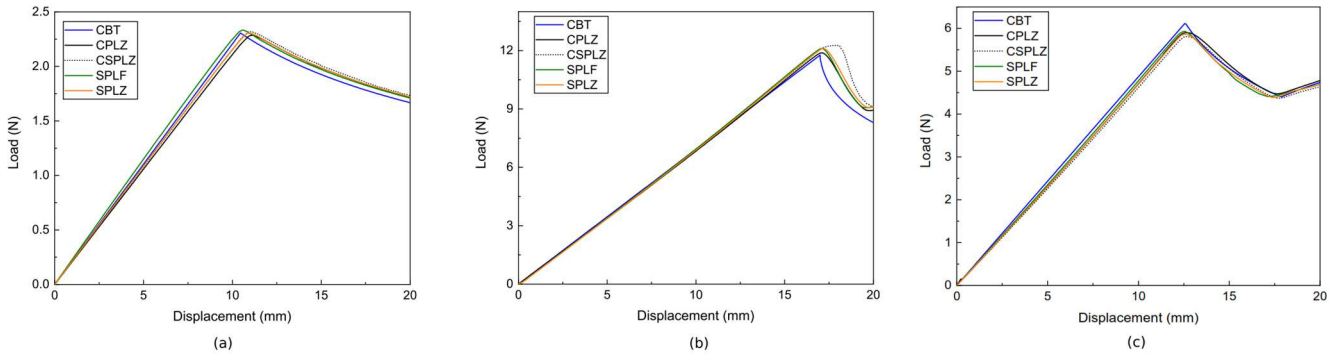

Fig. 3. The load-displacement curve of the (a) DCB, (b) ENF, and (c) SLB set-ups for different ply-level models as well as the CBT results.

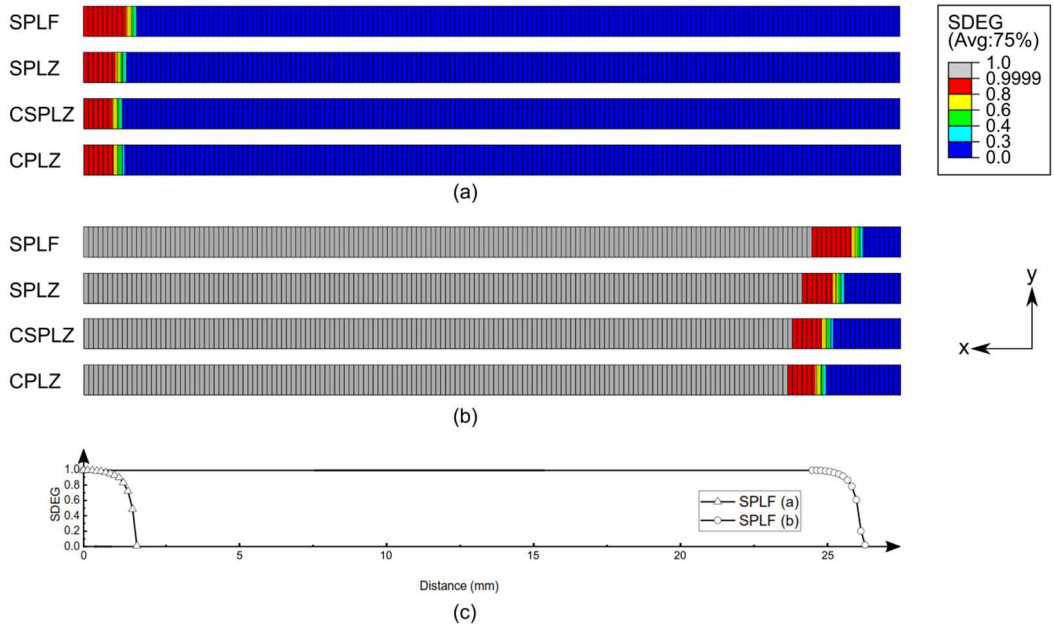

Fig. 4. Process zones and delamination areas of the SLB simulations at (a) the maximum load and (b) the end of the loading event. (c) shows the SDEG of the SPLF model at (a) and at (b) along x-direction.

The delamination areas of all models for the DCB, ENF, and SLB simulations exhibit very good agreement of the results for the entire delamination process. The state at the end of the loading event is reported in Table 3. The SPLF predicts a slightly larger delamination area than the other configurations in the context of DCB simulations. As illustrated in Fig. 3, the pre-peak stiffness of the SPLF model is slightly higher than other models, but delamination begins to propagate at a smaller applied displacement. This causes the differences in delamination area. Differently, the SPLF and SPLZ models are remarkably similar to those of the CPLZ reference model in the ENF and SLB simulations.

In terms of computational time, the model employing 3D continuum elements takes substantially longer to compute than the shell element-based ply-level models, as listed in Table 3. This phenomenon shows that the shell element-based ply-level models' system of equations is solved more efficiently than the continuum one. Furthermore, despite using the same conventional shell elements, the SPLZ model takes slightly longer to compute than the SPLF model. This is due to the varied coupling mechanisms used between the plies and the interface, as mentioned in Section 1. The results show that when applied to complex and large-scale laminated composite structures, the SPLF model can save a significant amount of computing time. Even better than for the DCB case, the SPLF model for the ENF case provides a very good tradeoff between reliable results and computational efficiency with roughly 10 minutes computation time. The SPLF model has a computation time that is 36 % lower than that of the SPLZ model. Again, the SPLF model remains the best one when compared to other models for SLB case. Furthermore, it is noted that one continuum element per ply thickness is considered to have lower accuracy compared to a shell element.

Table 3. The delamination area (mm^2) and the computation time (s) of DCB, ENF, and SLB simulations.

Ply-Level Models	Delamination Area (mm^2)			Computation Time (s)		
	DCB	ENF	SLB	DCB	ENF	SLB
CBT	15.38	20.10	22.95	-	-	-
CPLZ	14.37	20.10	23.11	1015	988	4337
CSPLZ	14.68	20.74	23.43	1172	1658	3046
SPLF	15.47	20.10	23.90	636	599	1812
SPLZ	14.68	20.10	23.59	739	943	2803

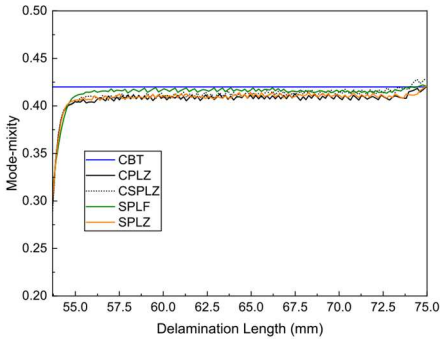

Fig. 5. The mode-mixity during delamination propagation of the SLB simulations setup.

3.3. Mode-mixity

Figure 5 shows the mode-mixity during delamination propagation from the initial delamination tip to the load point which is collected at the center of the element at the maximum displacement. The mode-mixity of the cohesive zone element is extracted by using the output variable of mode-mixity during damage evolution (MMIXDME). Initially, the value of MMIXDME is set to -1.0 (undamaged) before damage initiation and varies with time at a given integration point. However, the mode-mixity presented in this study is taken when the cohesive zone element is in critical conditions. The mode-mixity at the early transition phase suddenly increased. This phenomenon occurs until 2 mm distance when the process zone is completely formed (see Fig. 4(a)). Afterwards, the mode-mixity tends to be constant until the delamination reaches the load point. Generally, the mode-mixity of all ply-level based model are similar and provide close agreement with corrected beam theory results of 0.42. It should be highlighted that the mode-mixity value at around 0.42 shows that the SLB tests lead to mixed mode evolution in the interface.

4. Conclusions

A simulation technique based on cohesive zone elements was presented for evaluating progressive delamination in multilayered laminated composites by means of the Finite Element Method. Four different 3D ply-level modeling strategies were examined and compared in terms of delamination behavior such as load-displacement curves, delamination area, computation time, and mode-mixity during delamination propagation. Mode I, mode II, and mixed mode delamination were investigated using a double cantilever beam, end notch flexure, and single leg bending set-ups, respectively. All proposed models produced reliable findings when compared to the analytical results used as reference. The results showed that the ply-level approach based on shell elements in combination with finite thickness cohesive zone elements is the most favorable one in terms of accuracy of the result with low computational time. The model can also accurately predict the mixed mode behavior. Consequently, the implementation of this strategy can be particularly useful for predicting delamination behavior in complex and large-scale laminated composite structures.

Author Contributions

K. Anam planned the scheme, initiated the project, and conducted the numerical experiments; M. Todt analyzed the empirical results; H.E. Pettermann developed the mathematical modeling and examined the theory validation. The manuscript was written through the contribution of all authors. All authors discussed the results, reviewed, and approved the final version of the manuscript.

Acknowledgments

The Indonesian Ministry of Education, Culture, Research, and Technology (KEMDIKBUDRISTEK) and Österreichs Agentur für Bildung und Internationalisierung (OeAD-GmbH) in collaboration with ASEAN European Academic University Network (ASEA-UNINET) are gratefully acknowledged for sponsoring KA under Indonesia-Austria Scholarship Programme.

Conflict of Interest

The authors declared no potential conflicts of interest concerning the research, authorship, and publication of this article.

Funding

The authors received no financial support for the research, authorship, and publication of this article.

Data Availability Statements

The datasets generated and/or analyzed during the current study are available from the corresponding author on reasonable request.

Nomenclature

a	Delamination length [mm]	N'	Correction factor
B	Width [mm]	P_i	Load (i = I, II, m) [N]
E_i	Young's modulus (i = x, y, z) [N/mm^2]	t_i	Traction (i = n,s) [N/mm^2]
F	Correction factor	δ_i	Separation (i = I, II, m) [mm]

G_i	Shear modulus [N/mm^2]	ε_{yy}	Strain
$\mathcal{G}_i$	Strain energy release rate (i = I, II, IC, IIC) [N/mm]	χ	correction factor
h	Height [mm]	η	cohesive parameter
I	second moment of area [mm^4]	Γ	correction factor
K_i	stiffness (i = I, II) [N/mm^3]	γ	shear strain
L	Length [mm]	ν	Poisson's ratio
l_i	Element length (i = x, y, z) [mm]	ψ	mode-mixity

Appendix A. Corrected Beam Theory Equations

A.1. Mode I – DCB

Revisiting Fig. 2(a), the δ_{I} can be obtained by:

$$\delta_{\mathrm{I}} = \frac{2P_{\mathrm{I}}(a+\chi h)^3}{3E_{\mathrm{x}}I} \tag{A.1}$$

$$I = \frac{Bh^3}{12} \tag{A.2}$$

where I is the second moment of area along the beam length, E_{x} the Young's modulus of the beam, χ is the correction factor and h is the beam thickness [24, 25]. An analytical value of χ is defined as:

$$\chi = \sqrt{\frac{E_{\mathrm{x}}}{11G_{\mathrm{xz}}}\left[3-2\left(\frac{\Gamma}{1+\Gamma}\right)^2\right]} \tag{A.3}$$

and

$$\Gamma = 1.18\frac{\sqrt{E_{\mathrm{x}}E_{\mathrm{y}}}}{G_{\mathrm{xz}}} \tag{A.4}$$

where E_{y} and G_{xz} are transverse Young's and transverse shear modulus, respectively. Moreover, the $\mathcal{G}_{\mathrm{I}}$ is given by [26]:

$$\mathcal{G}_{\mathrm{I}} = \frac{P_{\mathrm{I}}^2(a+\chi h)^2}{BE_{\mathrm{x}}I} \tag{A.5}$$

During delamination propagation, the load-displacement response and the delamination extension can be obtained by combining Equations (A.1) and (A.5) and set the $\mathcal{G}_{\mathrm{IC}}$ instead of $\mathcal{G}_{\mathrm{I}}$.

A.2. Mode II – ENF

Revisiting Fig. 2(b), the δ_{II} can be obtained by:

$$\delta_{\mathrm{II}} = \frac{3P_{\mathrm{II}}(a+0.42\chi h)^3 \ + \ 2P_{\mathrm{II}}L^3}{96E_{\mathrm{x}}I} \tag{A.6}$$

where δ_{II} is the central displacement. Moreover, the $\mathcal{G}_{\mathrm{II}}$ can be defined as:

$$\mathcal{G}_{\mathrm{II}} = \frac{3(a \ + \ 0.42\chi h)^2P_{\mathrm{II}}^2}{64BE_{\mathrm{x}}I} \tag{A.7}$$

The load-displacement response and the delamination extension during delamination propagation can be obtained by combining Equations (A.6) and (A.7) and set the $\mathcal{G}_{\mathrm{IIC}}$ instead of $\mathcal{G}_{\mathrm{II}}$.

A.3. Mixed-mode I/II – SLB

Revisiting Fig. 2(c), the central displacement, δ_{m}, as well as $\mathcal{G}_{\mathrm{I}}$ and $\mathcal{G}_{\mathrm{II}}$ are given by [27] as:

$$\delta_{\mathrm{m}} = \frac{P_{\mathrm{m}}N'[7(a \ + \ 0.42\chi h)^3+(L+2\chi h)^3]}{2Bh^3E_{\mathrm{x}}} \tag{A.8}$$

$$\mathcal{G}_{\mathrm{I}} = \frac{3FP_{\mathrm{m}}^2(a \ + \ \chi h)^2}{B^2h^3E_{\mathrm{x}}} \tag{A.9}$$

$$\mathcal{G}_{\mathrm{II}} = \frac{9FP_{\mathrm{m}}^2(a \ + \ 0.42\chi h)^2}{4B^2h^3E_{\mathrm{x}}} \tag{A.10}$$

where F and N' are correction factors for large displacements. In this study, N' is set as ψ while F is calculated by using equation from [27]. The analytical load, P_{m}, at which delamination propagation begins was calculated using the BK criterion given by Eq. (2).

References

[1] Brunner, A.J., Murphy, N., Pinter, G., Development of a standardized procedure for the characterization of interlaminar delamination propagation in advanced composites under fatigue mode I loading conditions, *Engineering Fracture Mechanics*, 76, 2009, 2678–2689.
[2] Camanho, P.P., Davila, C.G., Moura, M.F.D., Numerical simulation of mixed-mode progressive delamination in composite materials, *Journal of*

Composite Materials, 37, 2003, 1415–1438.
[3] Bae, H.S., Kang, M.S., Woo, K.S., Kim, I.G., In, K.H., Test and analysis of modes I, II, and mixed-mode I/II delamination for carbon/epoxy composite laminates, *International Journal of Aeronautical and Space Sciences*, 20, 2019, 636–652.
[4] Rarani, M.H., Sayedain, M., Finite element modeling strategies for 2D and 3D delamination propagation in composite DCB specimens using VCCT, CZM, and XFEM approaches, *Theoretical and Applied Fracture Mechanics*, 103, 2019, 1–10.
[5] Ceglar, T., Schwab, M., Pettermann, H.E., DCB and ENF multi-scale simulations, *6th ECCOMAS Thematic Conference on the Mechanical Response of Composites: COMPOSITES 2017*, Editor: J.J.C. Remmers, A. Turon, TU Eindhoven, 2017.
[6] Dugdale, D., Yielding of steel sheets containing slits, *Journal of the Mechanics and Physics of Solids*, 8, 1960, 100–104.
[7] Barenblatt, G., The mathematical theory of equilibrium cracks in brittle fracture, *Advances in Applied Mechanics*, 7, 1962, 55–129.
[8] Turon, A., Camanho, P.P., Costa, J., Renart, J., Accurate simulation of delamination growth under mixed-mode loading using cohesive elements: Definition of interlaminar strengths and elastic stiffness, *Composite Structures*, 92, 2010, 1857–1864.
[9] Schwab, M., Todt, M., Wolfahrt, M., Pettermann, H.E., Failure mechanismbased modeling of impact on fabric reinforced composite laminates based on shell elements, *Composites Science and Technology*, 128, 2016, 131–137.
[10] Lindgaard, E., Bak, B.L.V., Glud, J.A., Sjølund, J., Christensen, E.T., A user programmed cohesive zone finite element for ansys mechanical, *Engineering Fracture Mechanics*, 180, 2017, 229–239.
[11] Dang, Z., Cao, J., Pagani, A., Zhang, C., Fracture toughness determination and mechanism for mode-I interlaminar failure of 3D-printed carbon Kevlar composites, *Composites Communications*, 39, 2023, 101532.
[12] Needleman, A., A continuum model for void nucleation by inclusion debonding, *Journal of Applied Mechanics*, 54, 1987, 525–531.
[13] Hillerborg, A., Modéer, M., Petersson, P.E., Analysis of crack formation and crack growth in concrete by means of fracture mechanics and finite elements, *Cement and Concrete Research*, 6, 1976, 773–781.
[14] Heidari-Rarani, M., Sayedain, M., Finite element modeling strategies for 2D and 3D delamination propagation in composite DCB specimens using VCCT, CZM, and XFEM approaches, *Theoretical and Applied Fracture Mechanics*, 103, 2019, 102246.
[15] Anam, K., Todt, M., Pettermann, H.E., Computationally efficient modeling of delamination behavior in laminated composites, *8th ECCOMAS Thematic Conference on the Mechanical Response of Composites: COMPOSITES 2021*, Editor: M. Fagerström, G. Catalanotti, Chalmers University of Technology, 2021.
[16] Dassault Systemes Simulia Corp., Providence, RI, USA, Abaqus Analysis User's Guide, Release 2020, 2020.
[17] Carlsson, L., Gillespie, J., Pipies, R., On the analysis and design of the end notched flexure (ENF) specimen for mode II testing, *Journal of Composite Materials*, 20, 1986, 594–604.
[18] Davies, P., Casari, P., Carlsson, L., Influence of fibre volume fraction on mode II interlaminar fracture toughness of glass/epoxy using the ENF specimen, *Composites Science Technology*, 65, 2005, 295–300.
[19] Gager, J., Pettermann, H.E., FEM modeling of multilayered textile composites based on shell elements, *Composites Part B: Engineering*, 77, 2015, 46–51.
[20] Springer, M., *Nichtlineare Finite Elemente Simulation der Schädigungsmechanismen sowie der Resttragfähigkeit von Schlagbeanspruchten Kohlenstofffaser-Epoxidharz-Verbunden*, Master Thesis, TU Wien, ILSB, Vienna, Austria, 2014.
[21] Benzeggagh, M.L., Kenane, M., Measurement of mixed-mode delamination fracture toughness of unidirectional glass/epoxy composites with mixed-mode bending apparatus, *Composite Science and Technology*, 56, 1968, 439–449.
[22] Hadavinia, H., Ghasemnejad, H., Effects of mode-I and mode-II interlaminar fracture toughness on the energy absorption of CFRP twill/weave composite box sections, *Composite Structures*, 89, 2009, 303–314.
[23] Falk, M.L., Needleman, A., Rice, J.R., A critical evaluation of cohesive zone models of dynamic fracture, *Journal de Physique IV, Proceedings*, 11, 2001, 543–550.
[24] Harper, P.W., Hallett, S.R., Cohesive zone length in numerical simulations of composite delamination, *Engineering Fracture Mechanics*, 75, 2008, 4774–4792.
[25] Hashemi, S., Kinloch, A., Williams, J., The analysis of interlaminar fracture in uniaxial fibre-polymer composites, *Proceedings of the Royal Society of London*, 427, 1990, 173–199.
[26] Reeder, J.R., Demarco, K., Whitley, K.S., The use of doubler reinforcement in delamination toughness testing, *Composites Part A: Applied Science and Manufacturing*, 35, 2004, 1337–1344.
[27] Kinloch, A.J., Wang, Y., Williams, J.G., Yayla, P., The mixed-mode delamination of fibre composite materials, *Composites Science and Technology*, 47, 1993, 225–237.

ORCID iD

Khairul Anam https://orcid.org/0000-0002-8588-9528
Melanie Todt https://orcid.org/0000-0002-5599-6373
Heinz E. Pettermann https://orcid.org/0000-0001-7162-5989

© 2024 Shahid Chamran University of Ahvaz, Ahvaz, Iran. This article is an open access article distributed under the terms and conditions of the Creative Commons Attribution-NonCommercial 4.0 International (CC BY-NC 4.0 license) (http://creativecommons.org/licenses/by-nc/4.0/).

How to cite this article: Anam K., Todt M., Pettermann H.E. An Efficient Ply-Level Based Modeling Strategy for Predicting Delamination Behavior in Laminated Composites, *J. Appl. Comput. Mech.*, 10(4), 2024, 652-658.
https://doi.org/10.22055/jacm.2024.45493.4377

Publisher's Note Shahid Chamran University of Ahvaz remains neutral with regard to jurisdictional claims in published maps and institutional affiliations.